J|A|C|S
ARTICLES
Published on Web 03/22/2002

Variable-Temperature Nuclear Magnetic Resonance Spectroscopy Allows Direct Observation of Carboxylate Shift in Zinc Carboxylate Complexes

Alojz Demšar,* Janez Košmrlj, and Saša Petriček

Contribution from the Faculty of Chemistry and Chemical Technology, University of Ljubljana, Aškerčeva 5, SI-1000 Ljubljana, Slovenia

Received July 2, 2001

Abstract: Tetranuclear complexes $[Zn_4(bdmap)_2(OOCR)_6]$ **1** (R = Me) and **2** (R = Et), where Hbdmap = 1,3-bis(dimethylamino)-2-propanol, were prepared from zinc carboxylates and Hbdmap in tetrahydrofuran (THF). The solid-state structures of isomers **1a** and **2a** consist of two pairs of zinc atoms, each bridged by two μ-1,2 and one μ-1,1 carboxylate ligands. Two pairs are connected by two tridentate bdmap ligands with oxygen acting as a bridging donating atom. The complexes retain the tetranuclear structure in solution and two dynamic processes are observed from variable-temperature ^{1}H and ^{13}C NMR spectra. A low-temperature process (LT dynamics) observed already below 200 K is a coalescence of the μ-1,2 and the μ-1,1 resonances to a single resonance. An additional dynamic process (HT dynamics) is observed above 247 K (**1**) and 263 K (**2**), leading to a coalescence of two dimethylamino resonances. Both dynamic processes are rationalized by a mechanism involving changes in the carboxylate coordination mode termed as carboxylate shift. The LT dynamics is ascribed to interconversions of a single μ-1,2 and a single μ-1,1 carboxylate ligation by rotations of 60°. The interconversions involve all carboxylate ligands in **1** and **2**. The HT dynamics is ascribed to the exchange of the coordinating geometries of two carboxylate-bridged zinc atoms. We propose a mechanism that starts with a cleavage of the Zn−N coordination bond. The resulting coordinatively unsaturated zinc atom acquires an additional oxygen donor atom by carboxylate shift of μ-1,2 carboxylate to μ-1,1 mode. The activation parameters ($\Delta H^{\ddagger}$ values in kilocalories per mole, $\Delta S^{\ddagger}$ values in calories per mole per kelvin) were determined by line-shape analysis of VT NMR spectra: for **1** in THF-d_8, $\Delta H^{\ddagger}_{LT} = 8.1(3)$, $\Delta S^{\ddagger}_{LT} = -12(2)$, $\Delta H^{\ddagger}_{HT} = 17.9(2)$, $\Delta S^{\ddagger}_{HT} = 14(1)$; for **1** in $CDCl_3$, $\Delta H^{\ddagger}_{HT} = 13.6(5)$, $\Delta S^{\ddagger}_{HT} = 3(3)$; for **1** in CD_2Cl_2, $\Delta H^{\ddagger}_{HT} = 9.9(3)$, $\Delta S^{\ddagger}_{HT} = -8(2)$; for **2** in THF-$d_8$, $\Delta H^{\ddagger}_{LT} = 11(1)$, $\Delta S^{\ddagger}_{LT} = -5(3)$, $\Delta H^{\ddagger}_{HT} = 19.6(5)$, $\Delta S^{\ddagger}_{HT} = 18(3)$. Polymeric $[Zn_4(bdmap)_2(OOCMe)_6]_n$ **1**-catena crystallizes from a dichloromethane solution of **1**. In **1**-catena, the zinc atoms are linked into a chain through μ-1,2 and μ-1,1 acetate alternated by μ-1,2 acetate and bdmap.

Introduction

Carboxylates are ligands in a wide range of polynuclear coordination compounds (including catalytic and biomimetic systems) and in metalloproteins.[1] They exhibit monodentate terminal, bidentate chelating, monodentate bridging (μ-1,1), and bidentate bridging (μ-1,2) coordination modes.[2] There is increasing X-ray structural and density functional theory (DFT) evidence that the altering of coordination mode, termed as a carboxylate shift, is a low-energy process that plays an important role in catalytic cycles of metalloenzymes.[3] The shifts along paths A, A′, B, and C (Scheme 1) were observed on diiron centers of soluble methane monooxygenase (MMO),[4] in R2 protein of ribonucleotide reductase (RNR-R2),[5] and in reactions of model compounds of diiron enzymes.[6]

The carboxylate coordination and its changes allow the structural flexibility of the bimetallic center and influence the

* Corresponding author. E-mail: alojz.demsar@uni-lj.si.

(1) For recent reviews, see (a) Sträter, N.; Lipscomb, W. N.; Klabunde, T.; Krebs, B. *Angew. Chem., Int. Ed. Engl.* **1996**, *35*, 2024−2055. (b) He, C.; Lippard, S. J. *J. Am. Chem. Soc.* **1998**, *120*, 105−113. (c) Ruttinger, W.; Dismukes, G. C. *Chem. Rev.* **1997**, *97*, 1−24. (d) Feig, A. L.; Lippard, S. J. *Chem. Rev.* **1994**, *94*, 759−805. (e) Lipscomb, W. N.; Sträter, N. *Chem. Rev.* **1996**, *96*, 2375−2433. (f) Wilcox, D. E. *Chem. Rev.* **1996**, *96*, 2435−2458. (g) Wallar, B. J.; Lipscomb, J. D. *Chem. Rev.* **1996**, *96*, 2625−2657. (h) Solomon, E. I.; Brunold, T. C.; Davis, M. I.; Kemsley, J. N.; Lee, S. K.; Lehnert, N.; Neese, F.; Skulan, A. J.; Yang, Y. S.; Zhou, J. *Chem. Rev.* **2000**, *100*, 235−349. (i) Mulliez, E.; Fontecave, M. *Coord. Chem. Rev.* **1999**, *186*, 775−793. (j) Que, L. *J. Chem. Soc., Dalton Trans.* **1997**, 3933−3940. (k) Steenhuis, J. J.; Hutchison, R. S.; Barry, B. A. *J. Biol. Chem.* **1999**, *274*, 14609−14616.

(2) Rardin, R. L.; Tolman, W. B.; Lippard, S. J. *New J. Chem.* **1991**, *15*, 417−430.

(3) (a) LeCloux, D. D.; Barrios, A. M.; Mizoguchi, T. J.; Lippard, S. J. *J. Am. Chem. Soc.* **1998**, *120*, 9001−9014. (b) Torrent, M.; Musaev, D. G.; Morokuma, K *J. Phys. Chem. B* **2001**, *105*, 322−327. (c) Herold, S.; Lippard, S. J. *Inorg. Chem.* **1997**, *36*, 50−58. (d) Voegtli, W. C.; Khidekel, N.; Baldwin, J.; Ley, B. A.; Bollinger, J. M.; Rosenzweig, A. C. *J. Am. Chem. Soc.* **2000**, *122*, 3255−3261.

(4) (a) Rosenzweig, A. C.; Nordlund, P.; Takahara, P. M.; Frederick, C. A.; Lippard, S. *J. Chem. Biol.* **1995**, *2*, 409−418. (b) Whittington, D. A.; Lippard, S. *J. Am. Chem. Soc.* **2001**, *123*, 827−838. (c) Dunietz, B. D.; Beachy, M. D.; Cao, Y. X.; Whittington, D. A.; Lippard, S. J.; Friesner, R. A. *J. Am. Chem. Soc.* **2000**, *122*, 2828−2839.

(5) (a) Logan, D. T.; Su, X. D.; Aberg, A.; Regnstrom, K.; Hajdu, J.; Eklund, H.; Nordlund, P. *Structure* **1996**, *4*, 1053−1064. (b) Andersson, M. E.; Hogbom, M.; Rinaldo-Matthis, A.; Andersson, K. K.; Sjoberg, B. M.; Nordlund, P. *J. Am. Chem. Soc.* **1999**, *121*, 2346−2352. (c) Hogbom, M.; Andersson, M. E.; Nordlund, P. *J. Biol. Inorg. Chem.* **2001**, *6*, 315−323.

(6) Feig, A. L.; Masschelein, A.; Bakac, A.; Lippard, S. J. *J. Am. Chem. Soc.* **1997**, *119*, 334−342.

Scheme 1

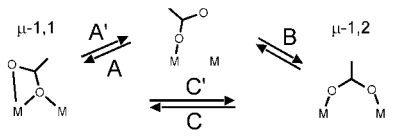

stability of the different oxidation states and electronic interaction between the two metal atoms at the active site.[7] The shifting glutamate in MMO alters the orientation of the protein helix and induces changes in the hydrogen-bonding network around the catalytic center.[4c] Additionally, the carboxylate-shift-like dynamics found with carbamate and hydroxamate ligands suggest that such processes could be a more general feature of other bidentate oxygen-donating ligands.[8]

Despite the carboxylate shift dynamic nature, until now, knowledge about it has only been acquired from solid-state structures and from theoretical calculations. Variable-temperature (VT) NMR spectroscopy could serve as a suitable technique for gathering information about carboxylate shift dynamics. In fact, separate resonances of μ-1,1 and μ-1,2 carboxylate ligands (CR_3COO^-; R = ^{1}H, ^{2}H, ^{19}F) have already been observed in ^{1}H, ^{2}H, and ^{19}F NMR spectra of nonfluxional paramagnetic bi- and polynuclear cobalt and iron complexes,[9] while in the fluxional complexes the resonances are broadened into the baseline.[10] On the other hand, only a single acetate resonance was reported for $[Zn_3(py)_2(OOCMe)_6]$ in solution, although its solid-state structure clearly exhibits two μ-1,1 and four μ-1,2 carboxylate ligands.[11] Studying the isomerization of metal complexes,[12] we report herein the first direct observation of carboxylate shift dynamics in tetranuclear complexes $[Zn_4(bdmap)_2(OOCR)_6]$ **1** (R = Me) and **2** (R = Et), where Hbdmap = 1,3-bis(dimethylamino)-2-propanol. The kinetics of the shift of coordinated carboxylates between μ-1,1 and μ-1,2 bridging modes (Scheme 1, path C and C′) was studied by VT ^{1}H and ^{13}C NMR spectroscopy, and mechanisms are proposed.

Results and Discussion

Syntheses and Crystal Structures. Compounds **1** and **2** were prepared as colorless crystals from zinc carboxylates and Hbdmap in THF. In the solid state they have tetranuclear centrosymmetric structures, as shown in Figures 1 and S1, which are denoted as isomers **1a** and **2a**. Two equatorial μ-1,2 carboxylate ligands are in the plane of four zinc atoms, and four apical (two μ-1,1 and two μ-1,2) carboxylate ligands are perpendicular to the plane. The dangling (uncoordinated) oxygen (O6) is at a distance of 2.841(9) Å (**1a**) or 2.797(7) Å (**2a**) to Zn2. Within each bdmap ligand, two -$CH_2N(CH_3)_2$ moieties

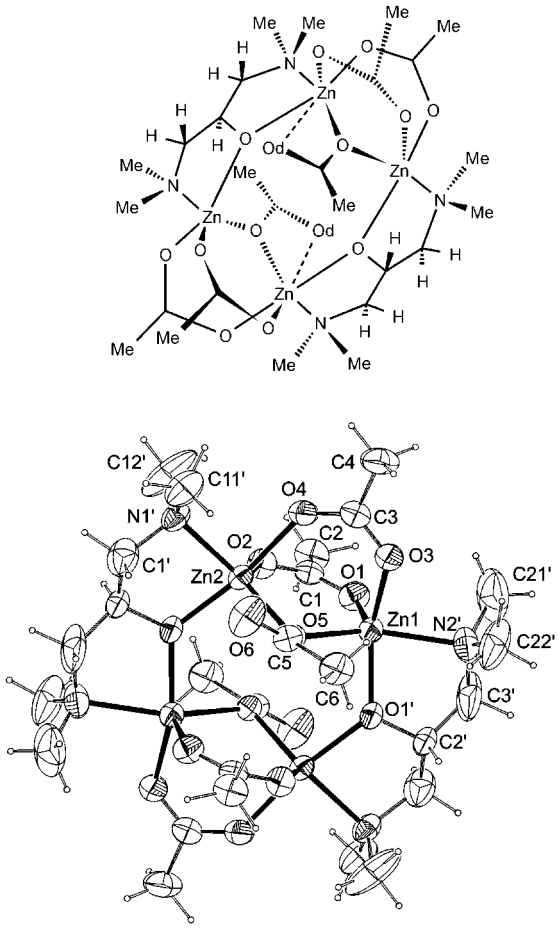

Figure 1. Molecular structure of **1a**. Distances in angstroms: Zn1−Zn2 3.215(1), Zn1−Zn2a 3.580(1), Zn1−O1 1.995(6), Zn1−O3 2.024(7), Zn1−N2′ 2.204(8), Zn2−O2 2.001(6), Zn2−O4 2.135(6), Zn2−N1′ 2.105(6), Zn1−O5 2.069(4), Zn2−O5 2.001(5). Representative torsion angles (in degrees): O(1′)−C(2′)−C(3′)−N(2′) = 34(2), O(1′a)−C(2′a)−C(1′)−N(1′) = 43.6(13).

differ in their geometries and in Zn−N coordinating distances, as can be seen from torsion angles and atomic distances in Figures 1 and S1. The ^{13}C cross-polarization/magic angle spinning (CP/MAS) spectrum of **1** (see Supporting Information) shows two dimethylamino resonances, ascribed to dimethylamino groups, coordinated to two nonequivalent carboxylate-bridged zinc atoms. The acetate carbons only appear as a single resonance.

Variable-Temperature NMR Studies. At temperatures below 212 K, the proton spectrum of **1** in THF-d_8 exhibits two carboxylate resonances in an intensity ratio of 2:1, ascribed to μ-1,2 and μ-1,1 coordinations, respectively (Figure 2). Two broad resonances at δ 2.29 and 2.36 belong to two dimethylamino groups, coordinated to two nonequivalent carboxylate-bridged zinc atoms. With the temperature increase, the carboxylate resonances between 222 and 232 K coalesce to a single resonance. This dynamic process is denoted as low-temperature (LT) dynamics. Additionally, during the temperature increase from 192 K, two broad dimethylamino resonances that initially show line sharpening start to broaden at 247 K, thus indicating an onset of an additional dynamic process. The dynamics, denoted as high-temperature (HT) dynamics, appears as a coalescence of two dimethyamino resonances at 282 K to a single peak. At higher temperatures, an additional sharpening

(7) (a) Dismukes, G. C. *Chem. Rev.* **1996**, *96*, 2909−2926. (b) Krebs, C.; Davydov, R.; Baldwin, J.; Hoffman, B. M.; Bollinger, J. M.; Huynh, B. H. *J. Am. Chem. Soc.* **2000**, *122*, 5327−5336.
(8) (a) Caudle, M. T.; Kampf, J. W. *Inorg. Chem.* **1999**, *38*, 5474−5475. (b) Arnold, M.; Brown, D. A.; Deeg, O.; Errington, W.; Haase, W.; Herlihy, K.; Kemp, T. J.; Nimir, H.; Werner, R. *Inorg. Chem.* **1998**, *37*, 2920−2925.
(9) (a) Hagen, K. S.; Lachicotte, R. J. *J. Am. Chem. Soc.* **1992**, *114*, 8741−8742. (b) Lachicotte, R.; Kitaygorodskiy, A.; Hagen, K. S. *J. Am. Chem. Soc.* **1993**, *115*, 8883−8884. (c) Hagen, K. S.; Lachicotte, R.; Kitaygorodskiy, A. *J. Am. Chem. Soc.* **1993**, *115*, 12617−12618. (d) Nair, V. S.; Hagen, K. S. *Inorg. Chem.* **1994**, *33*, 185−186. (e) Hagen, K. S.; Lachicotte, R.; Kitaygorodskiy, A.; Elbouadili, A. *Angew. Chem., Int. Ed. Engl.* **1993**, *32*, 1321−1324.
(10) Lachicotte, R. J.; Hagen, K. S. *Inorg. Chim Acta* **1997**, *263*, 407−414.
(11) Singh, B.; Long, J. R.; deBiani, F. F.; Gatteschi, D.; Stavropoulos, P. *J. Am. Chem. Soc.* **1997**, *119*, 7030−7047.
(12) Petriček, S.; Demšar, A.; Golič, L.; Košmrlj, J. *Polyhedron* **2000**, *19*, 199−204.

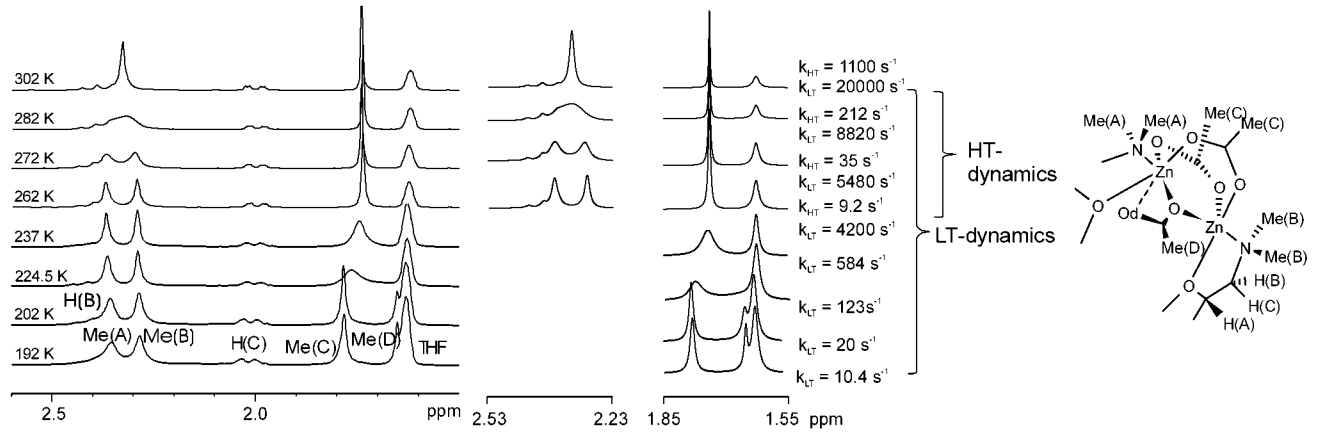

Figure 2. Observed (left) and simulated (right) VT ^{1}H NMR (300 MHz) of **1** in THF-d_8. See Supporting Information for complete set of spectra.

of carboxylate and dimethylamino resonances is observed. Analogous behavior is observed for THF-d_8 solution of **2** (Figure S2). At the temperatures up to 228 K, the proton spectrum shows two quartets (δ 2.02 and 1.92) in the intensity ratio of 2:1, ascribed to methylene ($CH_3CH_2COO^-$) protons of the carboxylates in μ-1,2 and μ-1,1 coordination modes. The coalescence to a single quartet is observed between 233 and 243 K (LT dynamics). The resonances of more distant methyl ($CH_3CH_2COO^-$) protons are less affected by carboxylate coordination. Two triplets (μ-1,2 and μ-1,1) are partially overlapped at 203 K ($\Delta\delta$ = 0.038 ppm) and coalesce above 233 K to one triplet resonance. Similarly to **1**, two dimethylamino resonances of **2** initially show line sharpening, then at 263 K start to broaden, and finally coalesce at 288 K (HT dynamics).

We also performed VT ^{1}H NMR analysis of **1** in $CDCl_3$ and CD_2Cl_2 solutions in order to study the solvent effect on solution dynamics (Figures S3 and S4, respectively). Both HT and LT dynamics were observed, though the acetate resonances at lower temperatures were not separated enough to allow line-shape analysis of spectra.

Similarly to the ^{13}C CP/MAS spectrum of **1**, the low-temperature ^{13}C NMR spectra of **1** in $CDCl_3$ and CD_2Cl_2 solution show two dimethylamino resonances with the acetate carbons appearing only as a single resonance. The dimethylamino resonances coalesce at 288 K ($CDCl_3$) and 272 K (CD_2Cl_2). The corresponding observed and simulated spectra are presented in Figures 3 and S5. A comparison of the rate constants obtained from VT ^{1}H NMR at coalescence temperatures with the rate constants obtained from VT ^{13}C NMR spectra at the same temperatures revealed that the process observed in VT carbon spectra is consistent with HT dynamics (the rate constants were obtained from line-shape analysis as discussed below).

(i) Mechanism of LT Dynamics. The possible mechanisms of LT dynamics with their corresponding simulated spectra in slow- and fast-exchange regimes along with the observed spectra of **1** are shown in Figure 4. The coalescence of μ-1,2 and μ-1,1 carboxylate resonances to the single resonance (LT dynamics), as observed in the VT ^{1}H NMR spectra, was rationalized by interconversions of diastereoisomers, differing in spatial distribution of four μ-1,2 and two μ-1,1 coordinated carboxylates.

Satisfactory fit of the observed spectra was possible only if all carboxylate ligands were involved in μ-1,2 $\leftrightarrow$ μ-1,1 coordination mode changes. This could be achieved by inter-

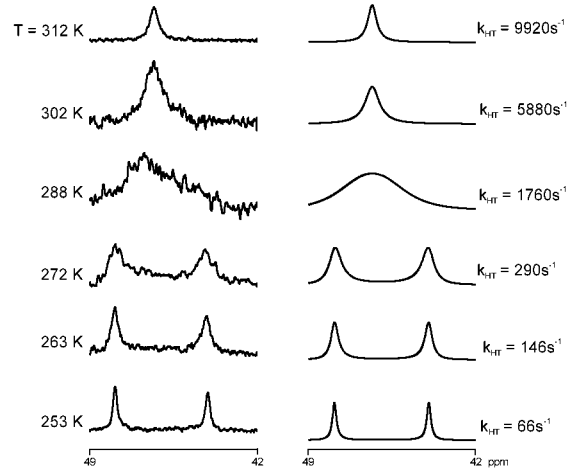

Figure 3. Observed (left) and simulated (right) dimethylamino resonances in variable-temperature ^{13}C NMR spectra of **1** (0.08 M solution in $CDCl_3$).

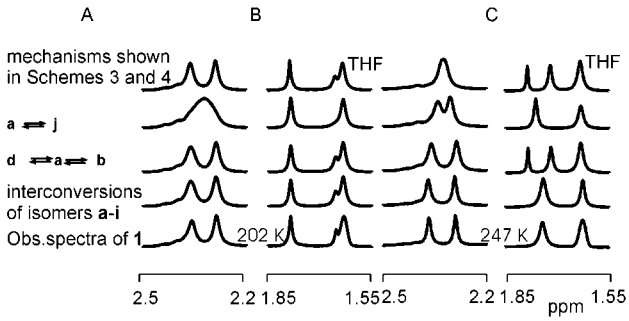

Figure 4. Considered mechanisms of LT dynamics (A), corresponding simulated ^{1}H NMR spectra in slow- (B, k_{LT} = 20 s^{-1}) and fast-exchange regimes (C, k_{LT} = 2000 s^{-1}), and the observed spectra of **1**.

conversions of isomers **a**−**i** (Chart 1). The set of isomers **a**−**i** differs in spatial distribution of four μ-1,2 and two μ-1,1 coordinated carboxylates, while two dangling oxygen atoms are at the same zinc atoms in all isomers. The mechanisms that leave some carboxylates unshifted (interconversions of isomers **a**, **b**, and **d** or of **a** and **j**) failed to model the observed VT ^{1}H NMR spectra. The simulation of spectra was also unsuccessful with the mechanisms that transfer the dangling oxygen atom from one to another carboxylate-bridged zinc atom (Schemes 3 and 4, mechanisms proposed for HT dynamics, see section ii).

The interconversions between isomers **a**−**i** can be achieved by rotation of two coordinated carboxylates by 60° around the

Chart 1. Schematic Presentation of Diastereoisomers That Interconvert by Proposed LT Dynamics

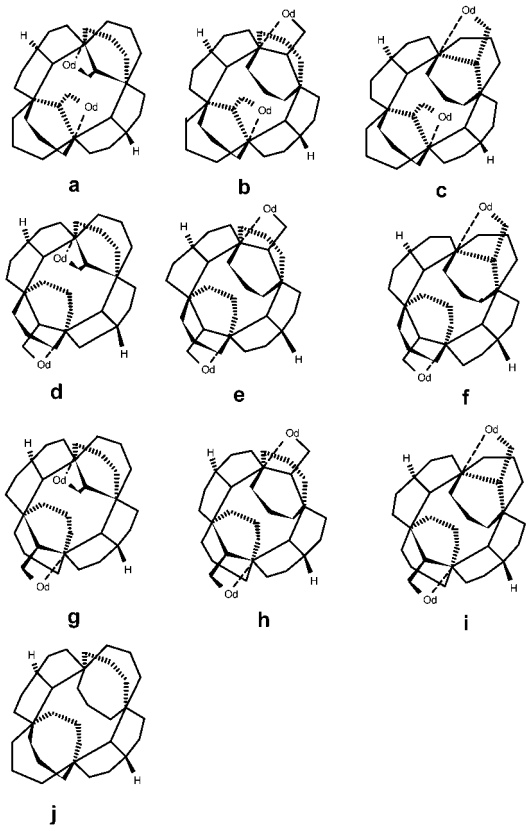

Scheme 2. Proposed LT Dynamics Interconversion of Two Isomers

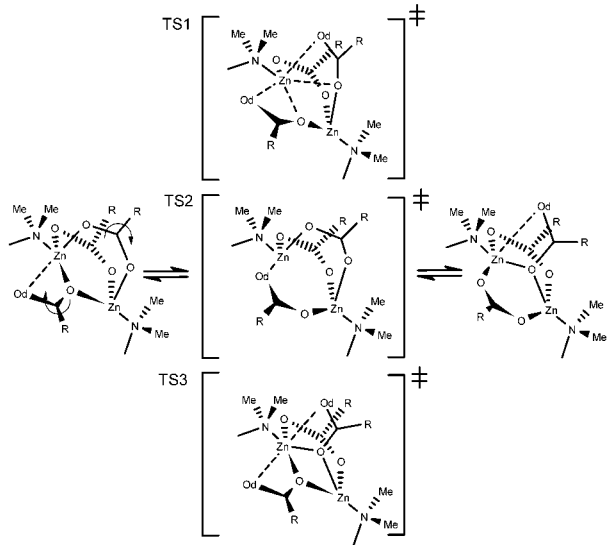

axis, normal to the -COO- plane, and passing through the carboxylic carbon atom, shown also in Scheme 2 by curved arrows. The rotation of μ-1,1 carboxylate brings the initially dangling (uncoordinated) oxygen (O_d) atom into proximity with the zinc, thus enabling its coordination to the metal atom. Additinally, the bidentate bridging oxygen shifts to the monodentate mode. The rotation of μ-1,2 carboxylate results in the reversed process: a departure of coordinated oxygen to the dangling position and the subsequent conversion of monodentate oxygen to the bidentate bridging mode. This hypothesis is based on two facts: the proximity of the dangling oxygen to Zn2 (O6 is an approaching atom in dynamics), and the relatively long Zn2−O4 distance (O4 is a leaving atom in dynamics) in crystal structures of **1a** and **2a**. In the next step, another pair of μ-1,1 and μ-1,2 carboxylates may perform an analogous exchange. Thus, taking into the account both pairs of zinc atoms, nine diastereoisomers **a**−**i** differing in the distribution of μ-1,1 and μ-1,2 carboxylates can be generated (Chart 1). For the rotation of carboxylates proposed in the above mechanism, three scenarios could be considered. (1) Rotation of both carboxylates in a concerted fashion via transition state $[TS1]^{\ddagger}$. The proposed transition state has two carboxylate ligands on the halfway between μ-1,2 and μ-1,1 coordination. The DFT study of carboxylate shift in the diiron system also revealed the transition state with such bonding of carboxylate ligand.[3b] (2) An initial rotation of μ-1,1 carboxylate into μ-1,2 mode through intermediate or transition state $[TS2]^{\ddagger}$, with the pair of zinc atoms bridged by three μ-1,2 carboxylates, (3) An initial rotation of μ-1,2 carboxylate via intermediate or transition state $[TS3]^{\ddagger}$, having the pair of zinc atoms bridged by two μ-1,1 and one μ-1,2 carboxylate. For $[TS2]^{\ddagger}$ a significant increase of distance between two carboxylate-bridged zinc atoms is required.[13] To the best of our knowledge, no data on isolated dizinc compounds having two μ-1,1 and one μ-1,2 bridging carboxylate (as in $[TS3]^{\ddagger}$) exist in the literature. Thus, if compared to $[TS2]^{\ddagger}$ and $[TS3]^{\ddagger}$, transition state $[TS1]^{\ddagger}$ is probably the lowest in energy and, hence, the most likely.

An exact simulation of ^{1}H NMR spectra of the mixture of interconverting diastereoisomers **a**−**i** could not be achieved. We assume that, even at slow interconversion rates, slightly different proton resonances of individual isomers are merged to a single μ-1,2 carboxylate resonance, a single μ-1,1 carboxylate resonance, and to two dimethylamino resonances. In principle, such merged resonances should show fast-exchange line sharpening by increasing the interconversion rate. In addition, both μ-1,2 and μ-1,1 carboxylate resonances should simultaneously broaden and then coalesce into a single resonance due to the exchange of coordination modes.

A simplified line-shape analysis of VT ^{1}H NMR spectra of **1** in THF-d_8 provided support for the mixture of interconverting diastereoisomers **a**−**i** in solution. We simulated ^{1}H NMR spectra by the approximation of carboxylate resonances with a single μ-1,2 and a single μ-1,1 carboxylate resonance (Figure 2, complete set of spectra in Figure S7). To be able to simulate the spectra, an optimization of the natural line width of resonances was necessary. A gradual decrease of natural line width of μ-1,2 resonance from $w_{1/2} = 3$ Hz (192 K) to $w_{1/2} = 0.6$ Hz (232 K) and μ-1,1 resonance from $w_{1/2} = 1$ Hz (192 K) to $w_{1/2} = 0.6$ Hz (232 K) was required (Figure S7). This is in agreement with the assumption that the carboxylate resonances are affected by simultaneous line sharpening and broadening. In addition, the mechanism is also supported by the fast-exchange line-width sharpening of both dimethylamino resonances (line width at 242 K is reduced to 60% of the line width at 202 K), and the onset of decoalescence of the merged μ-1,2 resonances observed at the $CH_3CH_2COO^-$ quartet in THF-d_8

(13) Zn−Zn distances of 3.465, 3.393, and 3.537 Å were found in tris(μ-1,2-alkylcarboxylate)-bridged complexes. See (a) Yamami, M.; Tanaka, M.; Sakiyama, H.; Koga, T.; Kobayashi, K.; Miyasaka, H.; Ohba, M.; Okawa, H. *J. Chem. Soc., Dalton Trans.* **1997**, 4595−4601. (b) Chan, W. H.; Mak, T. C. W.; Yip, W. H.; Kennard, C. H. L.; Smith, G.; Oreilly, E. J. *Aust. J. Chem.* **1987**, *40*, 981−986. (c) Birnbaum, A.; Cotton, F. A.; Dori, Z.; Kapon, M. *Inorg. Chem.* **1984**, *23*, 1617−1619.

Scheme 3. Proposed Dissociative Mechanisms of HT Dynamics of **1** and **2** and Mechanism of Polymerization of **1** to **1**-catena

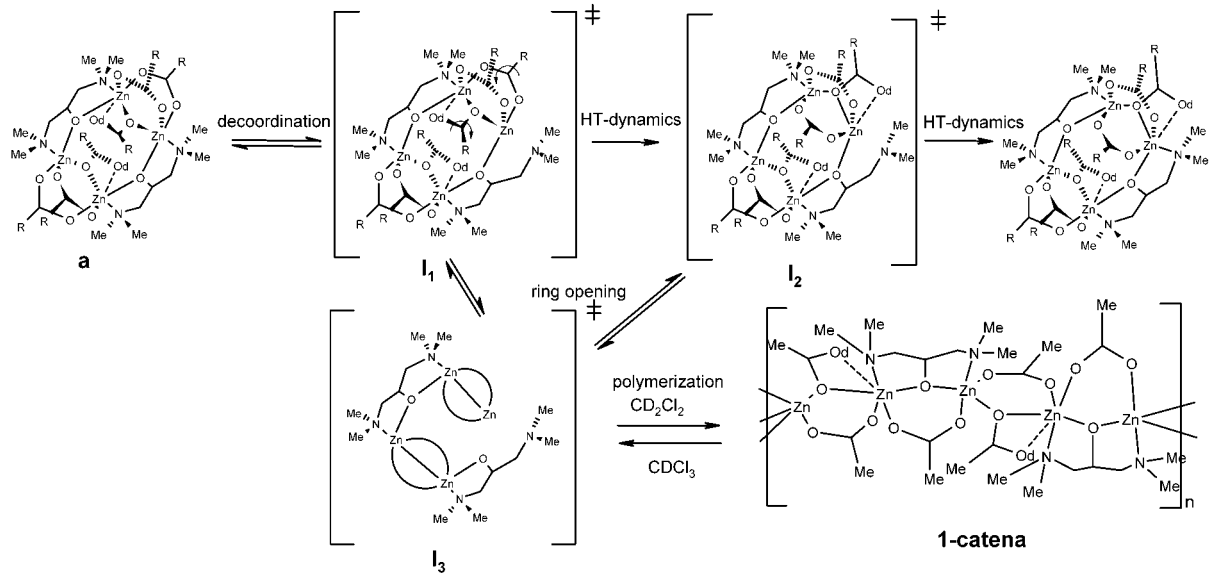

Scheme 4. Proposed Fluxional Mechanisms of HT Dynamics in **1** and **2**[a]

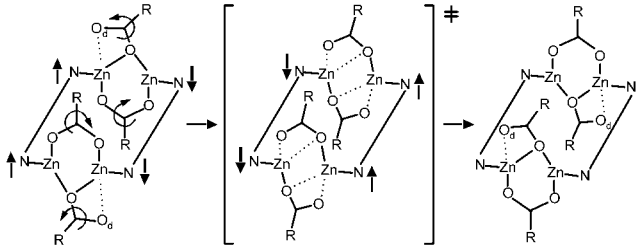

[a] Only carboxylates that shift are shown.

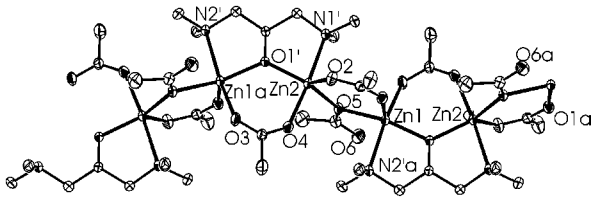

Figure 5. Structure of 1-catena·$2CD_2Cl_2$. Distances in angstroms: Zn1−Zn2 3.5808, Zn1−Zn2a 3.5269, Zn1−O1 2.0253, Zn1−O5 2.0849, Zn1−O1′b 2.0029, Zn1−O3b 2.0367, Zn1−N2′b 2.2571, Zn2−O1′ 1.9704, Zn2−O2 1.9936, Zn2−O4 2.0532, Zn2−O5 2.0063, Zn2−N1′ 2.2657. The solvate molecules are not shown.

solution of **2**. This resonance lost the quartet splitting upon cooling to 183 K (Figure S2).[14]

(ii) Mechanism of HT Dynamics. The behavior of bdmap resonances in VT ^{1}H and ^{13}C NMR spectra in the HT dynamics range is consistent with the averaging of two different $CH_2N(CH_3)_2$ moieties within the bdmap ligand. Several molecular processes could participate in this averaging:

(1) Dissociation of both Zn−N bonds within one bdmap, followed by the rotation of the ligand around the C−O axis for 180°. The energy barrier for this process should be high due to scission of two coordination bonds.

(2) Exchange of coordinating geometries between two carboxylate-bridged zinc atoms, as a result of transfer of the dangling oxygen atom from one carboxylate-bridged zinc atom to another zinc atom. The exchange achieved by μ-1,2 ↔ μ-1,1 interconversion of carboxylates influences the line shape of bdmap and carboxylate resonances. Several different pathways can be proposed for the exchange. (a) In a dissociative mechanism, an initial cleavage of the Zn−N bond (Scheme 3) yields an intermediate $[I_1]^‡$ with coordinatively unsaturated zinc atom, which then acquires an additional oxygen donor atom by μ-1,2 → μ-1,1 carboxylate shift. Consequently, another μ-1,1 carboxylate shifts to μ-1,2 mode to give $[I_2]^‡$. This mechanism is supported by the long Zn1−N2′ bond (dissociated bond) and short Zn1 to O4 (acquired oxygen) distance in the solid-state structures of **1a** and **2a** (see Supporting Information for distances). This process is then repeated at another pair of carboxylate-bridged zinc atoms. All isomers **a**−**i**, which interconvert by LT dynamics (Chart 1) should undergo analogous HT dynamics. (b) The same isomer as formed by dissociative mechanism is also accessible through the intermediate or transition state $[TS2]^‡$ (Scheme 2). The process is then repeated on another pair of carboxylate-bridged zinc atoms. (c) The fluxional mechanism is proposed as a wagging of the whole molecule resulting in a rotation of four apical carboxylates by 60° (Scheme 4).

The dissociative mechanism is strongly supported by the formation of $[Zn_4(bdmap)_2(OOCMe)_6]_n$ (**1**-catena, Scheme 3, Figure 5). The polymeric **1**-catena crystallizes from unsaturated CD_2Cl_2 or CH_2Cl_2/pentane solutions of **1** without concentrating or cooling of the solution (the analogous polymerization of **2** was not observed). Its formation can easily be explained by taking into the account the intermediates $[I_1]^‡$ and $[I_2]^‡$ of dissociative HT dynamics undergoing $Zn-O_{bdmap}$ bond cleavage (Scheme 3). The structure of **1**-catena·$2CD_2Cl_2$ (Figure 5) consists of a chain of zinc atoms alternatively bridged by μ-1,2 and μ-1,1 acetate or by μ-1,2 acetate and bdmap. The coordination geometry of zinc atoms in **1**-catena·$2CD_2Cl_2$ is similar to that in **1a**: two nonequivalent zinc atoms are five-coordinated with three carboxylate oxygens, one bdmap oxygen atom, and one amino nitrogen atom. The dangling oxygen (O6) is 2.708(3) Å from Zn1. The zinc−zinc distance of carboxylate-bridged atoms [3.5269(4) Å], which is longer than that in **1a** [3.215(1) Å], reflects two and three carboxylate bridges in **1**-catena and **1a**, respectively. The polymeric **1**-catena is very soluble in

(14) The μ-1,1 carboxylate resonance is not affected, ruling out the nonexchange broadening.

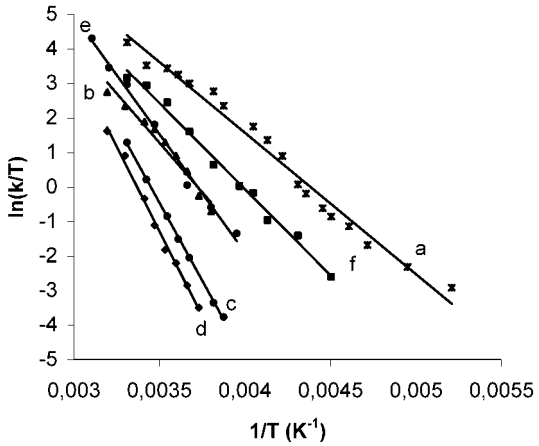

Figure 6. Eyring plots of dynamics, calculated from VT NMR spectra: (a) **1**, ^{1}H, THF-d_8, LT dynamics; (b) **2**, ^{1}H, THF-d_8, LT dynamics; (c) **1**, ^{1}H, THF-d_8, HT dynamics; (d) **2**, ^{1}H, THF-d_8, HT dynamics; (e) **1**, ^{13}C, $CDCl_3$, HT dynamics; (f) **1**, ^{13}C, CD_2Cl_2, HT dynamics.

$CDCl_3$. The ^{1}H NMR spectrum of the resulting solution is identical to the spectrum of **1**, showing that the tetrameric molecules are formed upon dissolving the polymeric **1**-catena in $CDCl_3$.

The methine and methylene protons of bdmap in **1** and **2** also show dynamic features in VT ^{1}H NMR spectra. The broad triplet C*H* resonance found in the LT dynamics range changes to a sharp triplet of triplets by HT dynamics. Similarly, the broad triplet and doublet assigned to two diastereotopic methylene protons change to a sharp triplet and doublet of doublets, respectively. These changes are in agreement with the resonances of two magnetically nonequivalent CH_2 groups in the bdmap ligand that are averaged by HT dynamics.

(iii) Kinetics of LT and HT Dynamics. The kinetic study of LT and HT dynamics was performed by line-shape analysis of VT NMR spectra. Spectra were simulated according to interconversions of isomers **a**−**i** for LT dynamics and dissociative mechanism for HT dynamics (Schemes 2 and 3).[15] The VT ^{1}H NMR spectra of **1** and **2** (THF-d_8) provided the rate constants of LT dynamics from the changes of carboxylate resonances. At higher temperatures the dimethylamino and carboxylate resonances were simulated by simultaneously running LT and HT dynamics (Figures 2, S7, and S8). The simulation of dimethylamino resonances in VT ^{13}C NMR spectra of **1** ($CDCl_3$ and CD_2Cl_2) provided rate constants of HT dynamics in these solvents (Figures 3 and S5).[16] The activation parameters were obtained from Eyring plots (Figure 6) and are summarized in Table 1.

Energy barriers of LT dynamics ($\Delta H^{\ddagger}_{LT}$) for **1** and **2** in THF-d_8 solution are 8.1(3) and 11(1) kcal mol^{-1}, respectively. For a rough evaluation of these values we used the results of the DFT study of μ-1,2 → μ-1,1 carboxylate shift in diiron model systems of MMO-R2.[3b] This conversion was calculated to be endothermic at 7.9 kcal mol^{-1}, and an additional energy barrier of 0.7 kcal mol^{-1} was calculated for the transition state. With these values for **1** and **2**, the estimated energy barrier for the proposed dynamics over transition state [TS1]‡ would be a sum of 8.6 kcal mol^{-1} (for μ-1,2 → μ-1,1 conversion) and 0.7 kcal mol^{-1} (for μ-1,1 → μ-1,2 conversion). Such an estimated energy barrier is in close agreement with the experimental activation enthalpy.

Table 1. Activation Parameters of Dynamics Calculated from VT NMR[a]

VT NMR spectra[b]	$\Delta H^{\ddagger}_{LT}$	$\Delta S^{\ddagger}_{LT}$	$\Delta G^{\ddagger}_{LT}$[c]	$\Delta H^{\ddagger}_{HT}$	$\Delta S^{\ddagger}_{HT}$	$\Delta G^{\ddagger}_{HT}$[c]
1, ^{1}H, THF-d_8	8.1(3)	−12(2)	11.7(9)	17.9(2)	14(1)	13.7(5)
2, ^{1}H, THF-d_8	11(1)	−5(3)	13(2)	19.6(5)	18(3)	15(1)
1, ^{13}C, $CDCl_3$	nd[d]	nd[d]	nd[d]	13.6(5)	3(3)	13(1)
1, ^{13}C, CD_2Cl_2	nd[d]	nd[d]	nd[d]	9.9(3)	−8(2)	13(1)

[a] $\Delta H^{\ddagger}$ and $\Delta G^{\ddagger}$ values are given in kilocalories per mole; $\Delta S^{\ddagger}$ values are given in calories per mole per kelvin; standard errors are in parentheses. [b] Refers to compound, NMR nucleus, and solvent, respectively. [c] At 298 K. [d] Not determined; only broadening of carboxylic ^{13}C resonance observed at low temperature.

The $\Delta H^{\ddagger}_{HT}$ and $\Delta S^{\ddagger}_{HT}$ values for HT dynamics of **1** and **2** are solvent-dependent. The high $\Delta H^{\ddagger}_{HT}$ relative to $\Delta H^{\ddagger}_{LT}$ ($\Delta H^{\ddagger}_{HT} \approx 2\Delta H^{\ddagger}_{LT}$) and high positive $\Delta S^{\ddagger}_{HT}$ values obtained for THF-d_8 solutions confirm the dissociative mechanism as the most plausible one.[17] On the other hand, compared to THF-d_8, significantly lower $\Delta H^{\ddagger}_{HT}$ and $\Delta S^{\ddagger}_{HT}$ values were obtained for $CDCl_3$ and CD_2Cl_2 solutions. This can be explained by a more extensive solvation of dissociated intermediate by chlorinated solvents than by THF. These results are also in agreement with the proposed dissociative mechanism. Namely, the enhanced solvation of dissociated zinc atom and amino nitrogen of intermediate $[I_1]^{\ddagger}$ retards the re-formation of the starting molecule from the intermediate $[I_1]^{\ddagger}$ and thus increases the intermediate concentration and the rate of HT dynamics.[18] The observation that **1**-catena·2CD_2Cl_2 is formed in CD_2Cl_2 solution of **1**, where the solvation of dissociated intermediate should be most effective according to kinetic parameters, also supports the dissociative mechanism.

IR Spectroscopy. The solid-state [poly(chlorotrifluoroethylene) mull] and pentachloroethanic solution IR spectra of **1** and **2** show absorption bands of asymmetric and symmetric carboxylate group vibrations (Figure 7). The bandwidth of asymmetric absorption in solid-state spectra is about half the bandwidth in solution spectra. The possible reasons for this broadening in solution could be solvation or the presence of isomers.

Conclusion

Two dynamic processes were observed and studied in solutions of **1** and **2** by VT NMR spectra. The LT dynamics was proposed as interconversion of very similar isomers by changing the carboxylate coordination mode. The activation parameters revealed a low energy barrier for this carboxylate shift process. The proposed mechanism of HT dynamics suggests that the change in metal coordination might cause a carboxylate shift. This process could be seen as a particular case of coupling of carboxylate shift and changes in coordination of noncarboxylate ligands to metal atoms proposed and observed

(15) Budzalaar, P. H. *gNMR;* Ivorysoft: Oxford, U.K., 1997.
(16) The line-shape analysis of VT ^{1}H NMR spectra of **1** in $CDCl_3$ and CD_2Cl_2 was not possible. The μ-1,2 and μ-1,1 acetate resonances are at low temperature not separated enough to allow the study of LT dynamics. The HT dynamics study of dimethylamino resonances was prevented due to the superposition of two dynamics: LT-dynamics sharpening and HT-dynamics broadening of the resonances.
(17) It is noteworthy that $\Delta H^{\ddagger}_{HT}$ in THF is in the range of coordination-bond energies; see Leininger, S.; Olenyuk, B.; Stang, P. J. Chem. Rev. **2000**, *100*, 853−908.
(18) The solvation of dissociated zinc atom of intermediate $[I_1]^{\ddagger}$ by THF and by chlorinated solvents could be assumed. The chlorinated solvents could, in addition, also solvate the amino nitrogen of intermediate $[I_1]^{\ddagger}$. (a) Kulawiec, R. J.; Crabtree, R. H. Coord. Chem. Rev. **1990,** *99*, 89−115. (b) Desiraju, G. R.; Steiner, T. *The Weak Hydrogen Bond*; Qxford University Press: Oxford, U.K., 1999; Chapter 2.

Table 2. Crystal Data and Experimental Details for **1a**, **2a**, and **1**-catena·$2CD_2Cl_2$

	1a	**2a**	**1**-catena·$2CD_2Cl_2$
chemical formula	$C_{26}H_{52}N_4O_{14}Zn_4$	$C_{32}H_{64}N_4O_{14}Zn_4$	$C_{26}H_{52}N_4O_{14}Zn_4{\cdot}2CD_2Cl_2$
cryst size (mm)	0.29 × 0.44 × 0.61	0.17 × 0.23 × 0.27	0.10 × 0.15 × 0.30
formula mass, g mol^{-1}	906.28	990.43	1080.10
collection *T*, K	293	293	200
(Mo Kα), Å	0.71073	0.71073	0.71073
cryst syst	monoclinic	monoclinic	monoclinic
space group	$P2_1/c$	$P2_1/c$	$P2_1/n$
a, Å	10.8650(10)	11.647(7)	10.7671(2)
b, Å	19.237(2)	19.630(10)	13.4855(3)
c, Å	10.0540(10)	10.178(2)	15.5292(4)
α, deg	90	90	90
β, deg	114.4420(10)	106.97(5)	90.7610(10)
γ, deg	90	90	90
V, Å^3	1913.1(3)	2225.7(19)	2254.64(9)
Z	2	2	2
ρ_{calc}, Mg/m^3	1.573	1.478	1.591
F(000)	936	1032	1104
θ range, deg	2.128.0	1.827.9	2.027.5
no. of collected reflns	18518	12749	9663
no. of indep reflns	4610	5293	5130
R_{int}	0.034	0.045	0.030
no. of reflns used	2487	1708	3879
no. of parameters	217	244	367
Goof	0.991	0.95	1.04
R^a [$I > 2.5\sigma(I)$]	0.061	0.042	0.040
$R_w{}^b$ or $wR_2{}^c$ [$I > 2.5\sigma(I)$]	0.073[b]	0.047[b]	0.088[c]
R (all data)	0.124	0.20	0.061
$R_w{}^b$ or $wR_2{}^c$ (all data)	0.184[b]	0.268[b]	0.099[c]
max/min res. electron density (e Å^3)	+0.94/−0.92	+1.26/−2.21	+0.61/−0.49

[a] $R = \Sigma(||F_o| - |F_c||)/\Sigma|F_o|$. [b] $R_w = \Sigma(w(||F_o| - |F_c||))/\Sigma(w|F_o|)$. [c] $wR_2 = (\Sigma[w(F_o^2 - F_c^2)^2]/\Sigma(wF_o^2)^2)^{1/2}$.

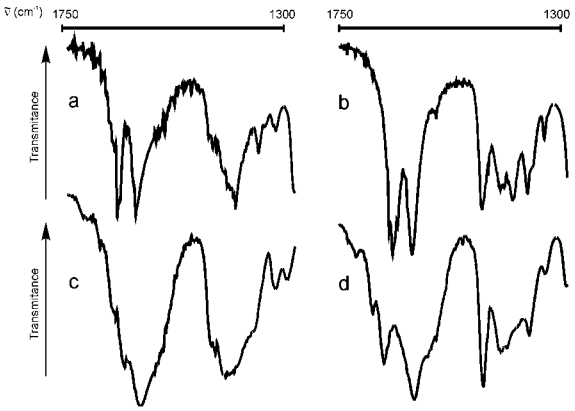

Figure 7. IR spectra in the range of asymmetric (at higher frequency) and symmetric (at lower frequency) carboxylate group vibrations: (a) **1**, solid; (b) **2**, solid; (c) **1**, solution; (d) **2**, solution.

in metalloprotein transformations.[2−5] These could provide new understanding of the role of carboxylate shift in carboxylate-coordinated active sites of metalloproteins as well as in related polynuclear metal catalysts.[19] New compounds with molecular topologies related to **1** and **2** may give an opportunity to study the role of metals and ligands in the carboxylate shift.

Experimental Section

General Considerations. ^{1}H and ^{13}C spectra were recorded at 300 and 75.4 MHz, respectively. ^{13}C cross-polarization/magic angle spinning (CP/MAS) spectra were recorded at 75.4 MHz. Solvent THF was dried with Na/K and distilled prior to use. The NMR solvents THF-d_8, $CDCl_3$, and CD_2Cl_2 were dried with CaH_2 and distilled prior to use. The spectra are referenced to Me_4Si.

(19) For a recent example of asymmetric aldol condensation with polynuclear zinc catalyst, see Trost, B. M.; Ito, H.; Silcoff, E. R. *J. Am. Chem. Soc.* **2001**, *123*, 3367−3368.

Synthesis of $[Zn_4(bdmap)_2(OOCCH_3)_6]$ (1). In a Schlenk flask, anhydrous $Zn(O_2CCH_3)_2$ (183 mg, 1 mmol) was suspended in THF (40 mL) and 1,3-bis(dimethylamino)-2-propanol (90 mg, 0.62 mmol) was added while the mixture was stirred. A clear solution resulted in 1 h. Colorless crystals grew from the solution during the slow evaporation of 30 mL of solvent at reduced pressure. The crystals were decanted, washed with cold THF (5 mL), and dried in vacuo for 10 min to give **1** (150 mg, 66%). Anal. Calcd for $C_{26}H_{52}N_4O_{14}Zn_4$: C, 34.36; H, 5.78; N, 6.18; Zn, 28.86. Found: C, 34.73; H, 5.65; N, 6.06; Zn, 28.6. IR [Nujol mull, poly(chlorotrifluoroethylene) mull] 2919, 1651, 1615, 1468, 1418, 1125, 1026, 999, 901, 865, 669, 611, 534 cm^{-1}. IR (solution in penthachloroethane, carboxylate absorptions) 1604, 1437 cm^{-1}. ^{1}H NMR ($CDCl_3$) δ 1.98 (s, 18H, $6CH_3CO_2^-$), 2.14 (dd, J = 11 and 3 Hz, 4H, $2CH_2^{equatorial}$), 2.43 (s, 24H, $4(CH_3)_2N$), 2.55 (t, J = 11 Hz, 4H, $2CH_2^{apical}$), 3.94 (tt, J = 11 and 3 Hz, 2H, 2CHO). ^{13}C NMR ($CDCl_3$) δ 22.0 ($CH_3CO_2^-$), 44.9 (CH_3N, $w_{1/2}$ = 60 Hz,), 61.6 (CHO), 64.1 (NCH_2), 178.1 ($CH_3CO_2^-$). ^{13}C CP/MAS (75.4 MHz): δ 25.4 ($CH_3CO_2^-$), 44.6, 48.5 (CH_3N), 63.6 (CHO), 66.6 (NCH_2), 177.7 ($CH_3CO_2^-$) (for ^{13}C CP/MAS spectrum, see also Figure S6).

Synthesis of $[Zn_4(bdmap)_2(OOCCH_3)_6]_n$ (1-catena). Pentane (5.7 mL) was added to the solution of **1** (180 mg) in CH_2Cl_2 (2 mL). The first tiny, regular-shaped crystals were observed to form after 5 h. Afer 2 days the solution was decanted and the crystals of **1**-catena (155 mg, 86%) were collected and dried in vacuo for 15 min. The crystals of **1**-catena·$2CD_2Cl_2$ used for X-ray crystallography were grown from 0.08 M CD_2Cl_2 solution of **1**. Anal. Calcd for $C_{26}H_{52}N_4O_{14}Zn_4$: C, 34.36; H, 5.78; N, 6.18; Zn, 28.86. Found: C, 34.71; H, 5.58; N, 5.99; Zn, 28.5. IR [Nujol mull, poly(chlorotrifluoroethylene) mull] 2924, 1647,-1614, 1419, 1303, 1125, 1027, 999, 901, 864, 668, 611, 534 cm^{-1}. ^{1}H NMR ($CDCl_3$) spectrum is identical to the spectrum of **1**.

Synthesis of $[Zn_4(bdmap)_2(OOCCH_2CH_3)_6]$ (2). Compound **2** was prepared analogously as described above for **1**, in 57% yield. Anal. Calcd for $C_{32}H_{64}N_4O_{14}Zn_4$: C, 38.81; H, 6.51; N, 5.66; Zn, 26.41. Found: C, 38.93; H, 6.43; N, 5.62; Zn, 26.4. IR [Nujol mull, poly-(chlorotrifluoroethylene) mull] 2970, 2834, 1644, 1606, 1468, 1432,

1407, 1379, 1298, 1253, 1124, 1080, 1032, 1000, 902, 884, 672, 536 cm^{-1}. IR (solution in penthachloroethane, carboxylate absorptions) 1616, 1601, 1465, 1431, 1375 cm^{-1}. ^1H NMR ($CDCl_3$) δ 1.01 (t, J = 7.5 Hz, 18H, $6CH_3CH_2$), 2.14 (dd, J = 11 and 3 Hz, 4H, $2NCH_2^{equatorial}$), 2.23 (q, J = 7.5 Hz, 12H, $6CH_3CH_2$), 2.44 (s, 24H, $4(CH_3)_2N$), 2.54 (t, J = 11 Hz, 4H, $2NCH_2^{apical}$), 3.94 (tt, J = 11 and 3 Hz, 2H, 2CHO). ^{13}C NMR ($CDCl_3$) δ 10.4 (CH_3CH_2), 29.5 (CH_3CH_2), 46.0 (CH_3N, $w_{1/2}$ = 80 Hz), 62.4 (CHO), 65.2 (NCH_2), 181.3 ($CH_2CO_2^-$).

X-ray Structure Determination and Refinement. Data for crystal structures of **1a** and **2a** were collected on an Enraf-Nonius CAD-4 four-circle diffractometer, and data for the structure of **1**-catena·$2CD_2Cl_2$ were collected on a Enraf-Nonius four-circle diffractometer equipped with a Kappa CCD area detector using Mo Kα radiation (α = 0.71074 Å). All the structures were solved by direct methods (SIR 92).[20] The structures of **1a** and **2a** were refined against F by use of Xtal3.4 system of crystallographic programs,[21] and the structure of **1**-catena·$2CD_2Cl_2$ against F^2 was refined by use of Shelxl-97.[22] A summary of crystal data of **1**, **2**, and **1**-catena is given in Table 2.

Acknowledgment. We thank Aleksandar Gačeša for the ^{13}C CP/MAS NMR spectrum and Drs. Janez Cerkovnik, Andrej Petrič, and Janez Plavec for helpful discussions. This work was supported by Grants PO-0511-0103 and PO-0503-0103 from the Ministry of Education, Science and Sport, Republic of Slovenia.

Supporting Information Available: Tables S1−S14 (crystallographic data of **1a**, **2a**, and **1**-catena·$2CD_2Cl_2$) and Figures S1 (ORTEP of **2a**), S2 (VT ^1H NMR of **2** in THF-d_8), S3 (VT ^1H NMR of **1** in $CDCl_3$), S4 (VT ^1H NMR of **1** in CD_2Cl_2), S5 (line-shape analysis of VT ^{13}C NMR of **1** in CD_2Cl_2), S6 (^{13}C CP/MAS spectrum of **1**), S7 (line-shape analysis of VT ^1H NMR of **1** in THF-d_8), and S8 (line-shape analysis of VT ^1H NMR of **2** in THF-d_8) (PDF). X-ray crystallographic data, in CIF format, are also available. This material is available free of charge via the Internet at http://pubs.acs.org.

JA016534X

(20) Altomare, A.; Cascarano, G.; Giacovazzo, C.; Guagliardi, A.; Burla, M. C.; Polidori, G.; Camalli, M. *J. Appl. Crystallogr.* **1994**, *27*, 435−436.
(21) Hall, S. R., King, G. S. D., Steward, J. M., Eds. *Xtal3.4 User's Manual*; University of Western Australia: Lamb, Perth, Australia, 1995.
(22) Sheldrick, G. M. *SHELX97: Program for the Refinement of Crystal Structures from Diffraction Data*; University of Göttingen: Göttingen, Germany, 1997.